Lattice mechanical study of the structure of dodecasil-3C

Lattice Mechanical Study of the Structure of Dodecasil-3C

A. J. M. de Man,† H. Küppers,‡ and R. A. van Santen*,†

Schuit Institute of Catalysis, Eindhoven University of Technology, P.O. Box 513, 5600 MB Eindhoven, The Netherlands, and Mineralogisches Institut, Universität Kiel, Kiel, FRG *(Received: May 29, 1991)*

A recently developed[1] partial charge potential model for SiO_2 polymorphs, derived from quantum chemical calculations, is applied to the calculation of the lattice energy minimized structure and physical properties of the low-density SiO_2 crystal Dodecasil-3C. Calculations are performed using Ewald summations and without symmetry constraints. Results are compared with calculations using the shell model of Sanders et at.[2,3] Best agreement between experimental and theoretically predicted elastic constants is achieved assuming a triclinic structure. In order to establish lattice stability, the vibrational frequency spectrum is calculated. For structures with imaginary frequencies, the corresponding atomic displacements are used to deform the quasi-stationary geometry. Upon lattice energy minimization, the deformed structure transforms to a stable energy minimum. Computation of thermal ellipsoids indicates that the large anisotropic temperature factors observed experimentally are mainly due to static disorder in atomic positions.

Introduction

The determination of the structure of complex synthetic (alumino-) silicates, like zeolites,[4] has become a topic of major interest because of their use as catalysts or molecular sieves. Since most zeolites cannot be synthesized as large single crystals, powder X-ray diffraction (XRD) or neutron diffraction[5] has to be used to clarify their structures. The complexity of the crystal unit cell, however, makes structure determination by powder diffraction only a difficult task and additional methods, like NMR[6], vibrational spectroscopy,[7-9] high-resolution electron microscopy,[10] sorption studies, and theoretical modeling,[11] have to be used. The combination of XRD with the DLS technique (distance least squares,[12] a modeling method to constrain the structure to meet distance and angle requirements) has become standard practice in zeolite structural chemistry. Crystal simulation methods using interatomic potentials have been applied extensively as well.[11,13-15] The advantage of the latter methods over DLS is that they are not restricted to calculating structures but are also able to compute vibrational spectra,[2,16,17] thermodynamic data,[18] and dielectric and elastic constants, i.e., empirical data that can be used to check the potentials independently from experimental structure determinations. In fact, previous determinations of Si-O potential parameters have partially been based on elastic constants[1,3] of α-quartz.

Recently elastic constants of a rather complex silica structure, Dodecasil-3C, a clathrasil[19-23] have been measured.[24] Since data on the elasticity of low-density SiO_2 polymorphs are virtually absent, comparison of these new experimental constants with theoretical values provides an interesting opportunity to verify the validity of potential parameters developed on the basis of studies on dense silica polymorphs.

Clathrasils are, like zeolites, porous tectosilicates with cages in which small molecules are enclosed during synthesis. The windows of the cages are too small for the molecules to leave. However, the cages are so large that small molecules can move almost unhindered inside the cage. The encapsulated molecules and the pure siliceous nature of the framework[20] distinguish the clathrasils from zeolites. Dodecasil-3C is isostructural with the highly siliceous "zeolite" ZSM-39 (structure type MTN).[25]

The composition of Dodecasil-3C is $34SiO_2 \cdot 4M^{12} \cdot 2M^{16}$. M^{12} are the guest molecules in the dodecahedral cages, usually N_2 or CH_4. M^{16} are larger molecules trapped in the hexadecahedral cages, such as pyrrolidine, adamantylamine, trimethylamine, etc. Depending on temperature and the nature of the guests, Dodecasil-3C exhibits several modifications. The high-temperature phase of Dodecasil-3C is cubic,[22,26] having space group $Fd\bar{3} = T_h^4 = 203$, with $a = 19.402$ Å. This phase is present above a transition temperature ranging between approximately 10 and 150 °C and shall be denoted Dodecasil-3C$_c$ in the following. A simplified picture of the Dodecasil-3C structure, showing only lines between the adjacent Si atoms, is given in Figure 1. As a consequence of dynamical and/or static disorder the Si-O distances reported in the X-ray structure analysis[22] are lower and the Si-O-Si angles are higher than the average values observed in silicates.[27,28] One of the Si-O-Si angles is 180° because all three atoms are constrained to lie on a 3-fold axis due to the cubic symmetry. Although the temperature factor of the oxygen atom involved is very high, the measured data did not allow a refinement of a structure with three split positions with occupation factors 1/3.

If the temperature is lowered, transitions to less symmetric phases take place. Chae et al.[29] observed for Dodecasil-3C with

† Eindhoven University of Technology.
‡ Universität Kiel.

(1) van Beest, B. W. H.; Kramer, G. J.; van Santen, R. A. *Phys. Rev. Lett.* **1990**, *64*, 1955.
(2) Sanders, M. J. Computer simulation of framework structured minerals. Ph.D. Thesis, University of London, 1984.
(3) Sanders, M. J.; Leslie, M.; Catlow, C. R. A. *J. Chem. Soc., Chem. Commun.* **1984**, 1271.
(4) Vaughan, D. E. W.; Treacy, N. M. J.; Newsam, J. M. In *Guidelines for mastering the properties of molecular sieves*; Barthomeuf, D., et al., Eds.; NATO ASI Series 221; Plenum: New York, 1990; p 99.
(5) Newsam, J. M. *Physica* B+C **1986**, *136*, 213.
(6) Klinowski, J. *Progr. NMR Spectrosc.* **1984**, *16*, 237.
(7) Flanigen, E. M.; Khatami, H.; Szymanski, H. A. *Adv. Chem. Ser.* **1971**, *101*, 201.
(8) Flanigen, E. M. In *ACS Monograph*; Rabo, J. A., Ed.; American Chemical, Society: Washington, D.C., 1976; Vol. 171, p 80.
(9) Dutta, P. K.; Shieh, D. C.; Puri, M. *Zeolites* **1988**, *8*, 306.
(10) Bursill, L. A.; Lodge, E. A.; Thomas, J. M. *Nature* **1980**, *286*, 111.
(11) Catlow, C. R. A.; Cormack, A. N. *Int. Rev. Phys. Chem.* **1987**, *6*, 227.
(12) Meier, W. M.; Villiger, H. *Z. Kristallogr.* **1969**, *129*, 411.
(13) Jackson, R. A.; Catlow, C. R. A. *Mol. Simul.* **1988**, *1*, 207.
(14) Jackson, R. A.; Bell, R. G.; Catlow, C. R. A. *Stud. Surf. Sci. Catal.* **1989**, *52*, 205.
(15) Parker, S. C.; Catlow, C. R. A.; Cormack, A. N. *Acta Crystallogr. B* **1984**, *40*, 200.
(16) de Man, A. J. M.; van Beest, B. W. H.; Leslie, M.; van Santen, R. A. *J. Phys. Chem.* **1990**, *94*, 2524.
(17) Kramer, G. J.; Farragher, N.; van Beest, B. W. H.; van Santen, R. A. *Phys. Rev. B* **1991**, *43*, 5068.
(18) Parker, S. C.; Price, G. D. In *Advances in Solid-State Chemistry*; Catlow, C. R. A., Ed.; JAI: London, 1989; Vol. 1, p 296.
(19) Gies, H. *Nachr. Chem., Tech. Lab.* **1985**, *33*, 387.
(20) Liebau, F.; Gies, H.; Gunawardane, R.; Marler, B. *Zeolites* **1986**, *6*, 373.
(21) Gies, H. *Z. Kristallogr.* **1986**, *175*, 93.
(22) Gies, H. *Z. Kristallogr.* **1984**, *167*, 73.
(23) Gies, H.; Liebau, F.; Gerke, H. *Angew. Chem.* **1982**, *94*, 214.
(24) Freimann, R.; Küppers, H. *Phys. Status Solidi A* **1991**, *123*, K123.
(25) Meier, W. M.; Olson, D. H. *Atlas of zeolite structure types*; Butterworth: London, 1987.
(26) Schlenker, J. L.; Dwyer, F. G.; Jenkins, E. E.; Rohrbaugh, W. J.; Kokotailo, G. T.; Meier, W. M. *Nature* **1981**, *294*, 340.
(27) Gibbs, G. V. *Am. Mineral.* **1982**, *67*, 421.
(28) Liebau, F. *Structural chemistry of silicates*; Springer: Berlin, 1985.
(29) Chae, H.; Klemperer, W.; Payne, D.; Suchital, C. T. A.; Wake, D. R.; Wilson, S. R. New Materials for Nonlinear Optics. *Clathrasils: New Materials for Nonlinear Optics*; ACS Symposium Series; American Chemical Society: Washington, DC, 1991.

0022-3654/92/2096-2092$03.00/0

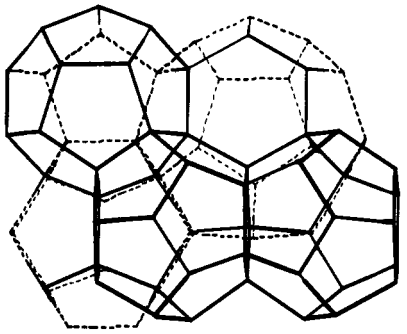

Figure 1. Structure of Dodecasil-3C,[22] showing four dodecahedral cages and a hexadecahedral cage (projected parallel to the dodecahedra layer and slightly tilted).

pyrrolidine as guest molecule a phase transition to a tetragonal phase which usually is accompanied with microtwinning. They succeeded in obtaining by chance a small single crystal which allowed an X-ray diffraction structure analysis. This modification, which shall be denoted here as Dodecasil-3C$_t$, has space group $I\bar{4}2d = D_{2d}^2 = 122$ with $a = 13.662$ Å and $c = 19.567$ Å. The tetragonal symmetry was also consistent with the ^{29}Si MAS NMR measurements of Fyfe et al.[30,31] Although some of the structure constraints are removed in the less symmetric space group, some of the Si–O–Si angles are still very high.

At even lower temperatures Dodecasil-3C further relaxes to less symmetric structures. X-ray powder diffraction patterns lead to orthorhombic, monoclinic, and triclinic unit cells.[32] A DLS refinement and a Rietveld refinement were done by Könnecke[32] in space group $Fddd = D_{2h}^{24} = 70$ with $a = 19.303$ Å, $b = 19.301$ Å, and $c = 19.494$ Å. This structure will be referred to as Dodecasil-3C$_o$.

We report the results of lattice energy minimizations using these three structures as starting structures. Emphasis is put on a comparison of computed and experimental elastic constants. Apart from this, it appears to be very useful to compute the vibrational frequencies of the structures obtained by energy minimization as well. For stable structures only real values of the frequencies are allowed. However sometimes imaginary frequencies are found, corresponding to saddle points in the multidimensional energy surface. The atomic displacements of the vibrational modes with an imaginary frequency can be used to generate new starting structures for the lattice energy minimization.

Methods and Models

The calculations are based on a classical description of the interatomic potentials in the crystal. Several potential types are used.

(a) The rigid ion potential of Catlow and co-workers[13] consisting of an electrostatic term using formal point charges on each ion, a short-range two-body interaction of the Buckingham[33] type, and an O–Si–O bond angle bending term. The electrostatic term is calculated for an infinite system using the Ewald summation technique, the short-range part is calculated for Si–O and O–O pairs with a distance of less than 10 Å, and the bending term is calculated for nearest neighbors only.

(b) The shell model of Sanders,[2,3] in which the polarizability of the oxygen ions is taken into account by considering them as a charged core (in which the atomic mass is concentrated) linked with a charged massless shell. The sum of the core and shell charges is the formal charge (−2), as in the rigid ion model. The short-range interactions are taken between shells.

(c) The SCF–empirical model of van Beest et al.[1,17] (here the name partial charge model is used). This is a rigid ion model using silicon charges of +2.4 and oxygen charges of −1.2. The model consists of two-body interactions only.

The potential parameters of the rigid ion and shell model are essentially based on fitting the structure of α-quartz, with an exception for the O–O term.[34] The partial charge model is obtained by a combined fitting on quantum chemical calculations of $Si(OH)_4$ molecules in various conformations and experimental data.[1,17]

The first step in modeling the cathrasil is the relaxation of the structure using the potentials given above. These studies were done without the trapped molecules. The relaxation consists of a minimization of the lattice energy of the system by changing the positions of the atoms as well as the unit cell vectors. No symmetry constraints are used, but the relaxation procedure tends to preserve symmetry to some extent. The relaxation program used, THBREL[35] (originating from the PLUTO code[36,37]), also calculates lattice properties like elastic constants and dielectric constants.

After the lattic energy minimization the phonon spectrum of the crystal is calculated. The calculation is performed in the harmonic approximation. Because we are mainly interested in infrared and Raman spectra, the phonon spectrum is calculated for a small wave vector (typically a 0.001 reciprocal unit cell vector). Spectral line intensities are calculated using the approximations of Kleinman and Spitzer,[38] and spectral line widths are assumed to be 10 cm^{-1}. More details are given in ref 16. Because of the limited success of the applied potential models in predicting spectra,[16] a general valence force field (GVFF)[39] is also used to calculate spectra. Since the GVFF cannot perform a structure relaxation, the structures that were obtained by the other potentials have been used.

The calculation of the thermal ellipsoids is done by a summation of the atomic displacement vectors for a representative set of phonon wave vectors. For atom i the mean square displacement matrix $\mathbf{U}_i$ is given by[40]

$$(\mathbf{U}_i)\alpha\beta = \sum_{\vec{k}} \sum_{j=1}^{3n} \frac{\hbar w_{\vec{k}}}{2M_i\omega_{(\vec{k};j)}} (\vec{v}_{(\vec{k};j;i)})_\alpha (\vec{v}_{(\vec{k};j;i)})_\beta \coth\left(\frac{\hbar\omega}{2k_BT}\right) \quad (1)$$

with $\vec{v}_{(\vec{k};j;i)}$ = atomic displacement vector of atom i for mode $(\vec{k};j)$, $\sum_{i=1}^{n}|\vec{v}_{(\vec{k};j;i)}|^2 = 1$; $\alpha, \beta = x, y, z$; n = number of atoms; $\vec{k}$ = wave vector; $w_{\vec{k}}$ = weight of wave vector (depending on integration method used), $\sum_k w_{\vec{k}} = 1$; $\omega_{(\vec{k};j)}$ = frequency of mode $(\vec{k};j)$; M_i = mass of atom i; k_B = Boltzmann constant; and T = temperature (273 K). The summation is done for N sample points in each direction using an "uneven" Brillouin zone sampling method of Filippini et al.[41] giving the components of the ith wave vector $\vec{k}_i$ as

$$(\vec{k}_i)_\alpha = \frac{1}{S}\left[\frac{1}{2}\left(\frac{i^2}{3+i^2}\right)^{1/3} + \sum_{j=1}^{i-1}\left(\frac{j^2}{3+j^2}\right)^{1/3}\right] \qquad i = 1, \ldots, N \quad (2)$$

with

$$S = \sum_{j=1}^{N}\left(\frac{j^2}{3+j^2}\right)^{1/3}$$

A grid of 9 × 9 × 9 points in the positive octant of the Brillouin zone was applied. The uneven sampling method was chosen in order to prevent divergence of U due to contributions from acoustic modes near the Brillouin zone center. No use of symmetry was

(30) Kokotailo, G. T.; Fyfe, C. A.; Gobbi, G. C.; Kennedy, G. J.; DeSchutter, C. T. *J. Chem. Soc., Chem. Commun.* **1984**, 1208.
(31) Fyfe, C. A.; Gies, H.; Feng, Y. *J. Chem. Soc., Chem. Commun.* **1989**, 1240.
(32) Könnecke, M. Private communication.
(33) Buckingham, R. A. *Proc. R. Soc. London, A* **1936**, *168*, 264.
(34) Catlow, C. R. A. *Proc. R. Soc. London, A* **1977**, *353*, 533.
(35) Leslie, M. *Daresbury Laboratory Technical Memorandum*, manuscipt in preparation.
(36) Catlow, C. R. A.; Mackrodt, W. C. *Computer simulation of solids*; Lecture Notes on Physics; Springer: Berlin, 1982.
(37) Catlow, C. R. A.; Doherty, M.; Price, G. D.; Sanders, M. J.; Parker, S. C. *Mater. Sci. Forum* **1986**, *7*, 163.
(38) Kleinman, D. A.; Spitzer, W. G. *Phys. Rev.* **1962**, *125*, 16.
(39) Etchepare, J.; Merian, M.; Smetankine, L. *J. Chem. Phys.* **1974**, *60*, 1873.
(40) Willis, B. T. M.; Pryor, A. W. *Thermal vibrations in crystallography*; Cambridge University Press: London, 1975.
(41) Filippini, G.; Gramaccioli, C. M.; Simonetta, M.; Suffritti, G. *Acta Crystallogr. A* **1976**, *32*, 259.

TABLE I: Atomic Distances and Angles, Unit Cell, Lattice Energy, and Elastic Constants of Cubic Dodecasil-3C$_c$

	experiment[22,24]	rigid ion	shell	partial charge
		Si–O Distances/Å		
Si1–O2	1.569	1.599	1.583	1.608
Si1–O1$^{2\times}$	1.574	1.605	1.586	1.606
Si1–O3	1.576	1.624	1.598	1.619
Si2–O4	1.546	1.579	1.569	1.594
Si2–O1$^{3\times}$	1.554	1.601	1.581	1.603
Si3–O4$^{4\times}$	1.526	1.582	1.568	1.590
av	1.566	1.604	1.585	1.606
		Si–O–Si Angles/deg		
T–O1–T	169.1	172.5	167.7	171.5
T–O2–T	177.8	178.9	178.8	179.0
T–O3–T	175.2	177.5	175.4	176.9
T–O4–T	180.0	180.0	180.0	180.0
av	174.5	176.5	174.3	176.1
		Unit Cell/Å		
a	19.402	19.893	19.627	19.918
		Lattice Energy/(kJ/(mol of SiO_2))		
E		−11 975.3	−12 402.9	−5591.60
		Elastic Constants (10^{11} dyn/cm^2)		
C_{11}	5.5	15.994	19.216	20.114
C_{12}	1.1	5.592	10.755	11.812
C_{44}	2.4	5.222	4.195	4.052
K_0	2.6	9.06	13.58	14.58
A	1.1	1.002	1.003	1.007

TABLE II: Atomic Distances and Angles of Tetragonal Dodecasil-3C$_t$

	experiment[29]	rigid ion	shell	partial charge
		Si–O Distances/Å		
Si1a–O3b	1.580	1.624	1.593	1.614
Si1a–O2c	1.586	1.599	1.604	1.610
Si1a–O1b	1.588	1.605	1.589	1.606
Si1a–O1d	1.590	1.605	1.592	1.608
Si1b–O2a	1.577	1.600	1.590	1.609
Si1b–O1d	1.590	1.605	1.592	1.605
Si1b–O3a	1.592	1.624	1.592	1.615
Si1b–O1c	1.593	1.605	1.598	1.605
Si1c–O2b	1.583	1.599	1.600	1.608
Si1c–O1a	1.583	1.605	1.591	1.603
Si1c–O1c	1.595	1.605	1.595	1.602
Si1c–O3b	1.596	1.624	1.594	1.616
Si2–O4	1.597	1.579	1.602	1.600
Si2–O2a	1.579	1.601	1.589	1.602
Si2–O2b	1.602	1.601	1.596	1.600
Si2–O2c	1.604	1.601	1.602	1.606
Si3–O4[4]	1.594	1.582	1.601	1.595
av	1.590	1.604	1.595	1.606
		Si–O–Si Angles/deg		
T–O1a–T	179.2	172.5	177.6	176.9
T–O1b–T	160.8	172.5	158.4	168.1
T–O1c–T	155.8	172.5	155.2	165.2
T–O1d–T	165.6	172.5	154.5	173.3
T–O2a–T	170.1	178.9	157.3	176.9
T–O2b–T	154.5	178.9	147.9	165.7
T–O2c–T	155.5	178.9	146.7	167.1
T–O3a–T	170.0	177.5	170.6	176.9
T–O3b–T	174.3	177.4	169.4	176.5
T–O4–T	146.2	180.0	142.7	158.9
av	162.0	176.5	156.1	169.9

made because relaxed structures were used.

For a simulation of ^{29}Si NMR spectra a simple empirical relation[42] between the chemical shift δ (in ppm relative to TMS) and the mean Si–O–Si angle per silicon atom was used:

$$\delta = -48.61 \sec(\overline{\text{Si–O–Si}}) - 168.04 \quad (3)$$

(42) Engelhardt, G.; Radeglia, R. *Chem. Phys. Lett.* **1984**, *108*, 271.

TABLE III: Unit Cell, Lattice Energy, and Elastic Constants of Tetragonal Dodecasil-3C$_t$

	experiment[29]	rigid ion	shell	partial charge
		Unit Cell/Å		
c	19.567	19.893	19.566	19.926
$2^{1/2}a/c$	0.9874	1.000	0.976	0.992
		Lattice Energy (kJ/(mol of SiO_2))		
E		−11 975.3	−12 406.9	−5591.9
		Elastic Constants/(10^{11} dyn/cm^2)		
C_{11}	5.7[a]	16.015	8.059	8.563
C_{12}	0.9[a]	5.571	1.042	0.465
C_{13}	1.1[a]	5.592	2.689	3.714
C_{33}	5.5[a]	15.994	12.292	14.557
C_{44}	2.4[a]	5.222	4.312	2.125
C_{66}	2.2[a]	5.201	2.921	4.068
K_0	2.6	9.06	4.25	4.46
A	1.1	1.002	1.645	1.710

[a] Experimental data originate from the cubic phase and are converted to a tetragonal setting rotated by 45° around [001].

TABLE IV: Atomic Distances and Angles of the Structures Deduced from Orthorhombic Dodecasil-3C$_o$

	DLS[32]	rigid ion	shell	partial charge
		Si–O Distances/Å		
Si1a–O1a	1.604	1.605	1.596	1.606
Si1a–O1b	1.604	1.605	1.591	1.606
Si1a–O2a	1.604	1.599	1.601	1.608
Si1a–O3c	1.604	1.624	1.597	1.613
Si1b–O2b	1.604	1.600	1.601	1.609
Si1b–O1b	1.605	1.605	1.596	1.604
Si1b–O3a	1.605	1.624	1.597	1.617
Si1b–O1c	1.613	1.605	1.591	1.603
Si1c–O1c	1.594	1.605	1.596	1.607
Si1c–O2c	1.605	1.599	1.601	1.608
Si1c–O1a	1.605	1.605	1.592	1.603
Si1c–O3b	1.605	1.624	1.597	1.614
Si2–O2b	1.590	1.600	1.599	1.600
Si2–O2a	1.590	1.601	1.599	1.606
Si2–O2c	1.590	1.601	1.599	1.602
Si2–O4	1.591	1.579	1.569	1.601
Si3–O4$^{4\times}$	1.586	1.582	1.568	1.596
av	1.600	1.604	1.594	1.606
		Si–O–Si Angles/deg		
T–O1a–T	156.6	172.5	155.7	178.2
T–O1b–T	156.7	172.5	155.7	172.1
T–O1c–T	157.7	172.6	155.7	160.8
T–O2a–T	146.9	178.9	147.5	167.6
T–O2b–T	146.6	178.9	147.5	166.0
T–O2c–T	146.0	178.9	147.5	175.8
T–O3a–T	177.0	177.5	177.5	174.7
T–O3b–T	175.3	177.5	177.5	176.0
T–O3c–T	176.2	177.5	177.5	174.8
T–O4–T	179.6	180.0	180.0	158.3
av	159.3	176.6	159.5	169.6

Spectral line widths of 0.5 ppm (fwhm) were used for all lines.

Experiment

The elastic constants were measured with the Brillouin scattering method from a cubic Dodecasil-3C single crystal at room temperature. Its cages contained N_2, Ar, and $N(CH_3)_3$. This latter, rather small guest molecule in the M^{16} cages enables the cubic structure to be stable even down to room temperature. More details can be found in ref 24. The infrared spectrum was measured at room temperature with the KBr pellet technique on a Bruker Model 113-v Fourier transform spectrophotometer at our laboratory using a pyrrolidine–Dodecasil-3C sample.

Results

The results of the lattice relaxation using the various potential models and starting from the three structures Dodecasil-3C$_c$, Dodecasil-3C$_t$, and Dodecasil-3C$_o$ are given in Tables I–V, re-

TABLE V: Unit Cell, Lattice Energy, and Elastic Constants of the Structures Deduced from Orthorhombic Dodecasil-3C$_o$

	DLS[32]	rigid ion	shell	partial charge
		Unit Cell/Å		
c	19.494	19.893	19.301	19.752
a/c	0.9902	1.0000	1.0000	1.0000
b/c	0.9901	1.0000	1.0000	1.0066
		Lattice Energy/(kJ/(mol of SiO_2))		
E		−11 975.3	−12 406.0	−5592.0
		Elastic Constants (10^{11} dyn/cm^2)[a]		
C_{11}	5.5	15.994	9.562	7.777
C_{33}		15.994	9.562	12.284
C_{12}	1.1	5.592	2.199	−0.042
C_{13}		5.592	2.199	2.097
C_{44}	2.4	5.222	3.116	3.250
C_{66}		5.222	3.116	3.973
K_o	2.6	9.06	4.65	3.61
A	1.1	1.002	1.086	1.597

[a] Because the relaxed structures have cubic or tetragonal symmetry only the independent elastic constants for a tetragonal unit cell are listed. The experimental values given originate from the cubic phase.

TABLE VI: Experimental and Calculated Elastic Constants of α-Quartz (10^{11} dyn/cm^2)

constant	experiment[57]	rigid ion	shell	partial charge
C_{11}	8.683	20.234	9.471	9.056
C_{33}	10.598	21.291	11.608	10.707
C_{12}	0.709	6.635	1.184	0.812
C_{13}	1.193	8.626	1.968	1.525
C_{44}	5.826	6.308	5.006	5.028
C_{14}	−1.806	0.000[a]	−1.452	−1.766
K_0	3.745	6.799	3.817	4.122

[a] The rigid ion model gives the structure of β-quartz. Experimental values of the elastic constants (10^{11} dyn/cm^2) for β-quartz are[58] C_{11} = 11.84, C_{33} = 10.70, C_{12} = 1.90, C_{13} = 3.20, and C_{44} = 3.585 (at 600 °C). Because of the hexagonal symmetry of β-quartz C_{14} = 0.

spectively. The bulk moduli K_0 are calculated without explicitly using symmetry from

$$\frac{1}{K_0} = \sum_{i=1}^{3}\sum_{j=1}^{3} s^{ij} \tag{4}$$

where s^{ij}, the compliance tensor, is the inverse of the elastic constant tensor C_{ij}. The anisotropy A of the elastic constants is given as

$$A = C_{max}/C_{min} \tag{5}$$

with C_{max} = maximum C'_{11} value for any direction and C_{min} = minimum C'_{11} value for any direction. A value of 1 indicates isotropy.

The lattice energies are very dependent on the potential parameters and should only be compared within the same potential model. As a reference, values calculated for α-quartz can be used. They are −11 956, −12 417, and −5628.9 kJ/(mol of SiO_2) for the rigid ion, shell, and partial charge models, respectively.

The structures that are relaxed from the cubic Dodecasil-3C$_c$ are still cubic and the symmetry is still $Fd\bar{3}$, so the 180° Si–O–Si angle is conserved. The largest structural change is an increase in Si–O bond length and a corresponding increase in unit cell length. In previous calculations with the same potential parameters on well-defined silica structures,[1,16,17] the shell model generally caused a slight decrease in unit cell dimension. From this it can be concluded that the Si–O bonds in Dodecasil-3C have to be larger than those derived from the experimental cubic structure refinement. A more significant discrepancy is the large difference between experimental and calculated elastic constants. This is in contrast to calculations on α-quartz and other dense silica polymorphs[1] that gave a better agreement between theoretical and experimental elastic constants, as is illustrated in Table VI.

The discrepancy in elastic constants diminishes substantially when the tetragonal structure of Chae et al. is used as the starting structure for a relaxation with the shell model as well as the partial charge model. This can be seen in Table III. The corresponding lattice energies are lower than when starting with cubic Dodecasil-3C$_c$, indicating a more stable structure. The rigid ion model, however, gives the same result as that in the cubic Dodecasil-3C$_c$ case. The distances and angles shown in Table II change more using the shell model than with the partial charge model. The shell model gives a tetragonally distorted structure while the partial charge model shows some tendency to give a cubic structure that is similar to the structure published by Gies. The symmetry of the shell model and partial charge model relaxed structures is still $I\bar{4}2d$. The elastic constants given by the shell model are in better agreement with experiment than those of the partial charge model.

TABLE VII: Average Si–O Distance, Average Si–O–Si Angle, Unit Cell, and Lattice Energy after Double Relaxation of Cubic Structure

	experimental	shell[a]	partial charge
		Si–O Distance/Å	
av	1.565	1.598	1.606
		Si–O–Si Angle/deg	
av	174.5	151.5	169.6
		Unit Cell/Å	
c	19.402	19.051	19.752
a/c	1.0000	1.0070	1.0000
b/c	1.0000	1.0044	1.0065
		Lattice Energy/(kJ/(mol of SiO_2))	
E		−12 408.1	−5592.0

[a] The shell model is triclinic with α = 89.47°, β = 89.87°, γ = 90.07°.

The orthorhombic structure given by Könnecke relaxes to the same cubic structure as the cubic and tetragonal structure when the rigid ion model is used (Tables IV and V). The shell model also results in a structure with cubic unit cell vectors. This one is more dense than the structure obtained when starting with cubic Dodecasil-3C$_c$. Its energy is significantly lower than that of the relaxed cubic structure but almost equal to that of the relaxed tetragonal one, although their structural properties differ. The elastic constants are worse, so for the shell model the tetragonal structure is preferable. The partial charge model results in a slightly tetragonal unit cell that is more dense than the one obtained from tetragonal Dodecasil-3C$_t$. The space group is $C2/c = C_{2h}^6$ = 15. The elastic constants agree somewhat better with experiment than those for the shell model.

The phonon spectra of the relaxed cubic structures contained imaginary frequencies, indicating that the structures are unstable because saddle points in the multidimensional energy surface have been found. For the shell model and partial charge model a further relaxation of the previous relaxed structures was made by adding to the atomic positions the vibrational displacements of the atoms corresponding to an imaginary mode. In the case of degenerate imaginary modes, all modes and their linear combinations with equal weights have been tested. The amplitude of the vectors added was about 0.1 Å. The unit cell vectors were not changed. The structures obtained is this way were relaxed again. The resulting structures will be designated Dodecasil-3C$_4$ (shell model) and Dodecasil-3C$_5$ (partial charge model). The properties of these "doubly" relaxed structures are given in Tables VII and VIII. The lattice energy of the shell model relaxed structure is lower than the lattice energies of the previous relaxed structures, and the elastic constants are better as well. The final unit cell is triclinic. The partial charge model relaxation results in the same unit cell vectors as those obtained from orthorhombic Dodecasil-3C$_o$. Also the lattice energies are comparable. The space group symmetry for the atomic positions of the doubly relaxed structures is shown in Table IX by means of the value χ that is defined as

$$\chi^2 = \frac{1}{nN}\sum_{i}^{N}\sum_{j}^{n} \min_{1\le k\le n} |\vec{r}_k - \mathbf{R}_i\vec{r}_j|^2 \tag{6}$$

with $\vec{r}_j$ = position of atom j in crystal coordinates (atoms j and k must be of the same type); $\mathbf{R}_i$ = ith symmetry operator of the

TABLE VIII: Elastic Constants after Double Relaxation of Cubic Structure

elastic constants/ (10^{11} dyn/cm^2)	experimental	shell[a]	partial charge
C_{11}	5.5	7.468	7.777
C_{22}		7.639	7.777
C_{33}		8.651	12.284
C_{12}	1.1	1.493	−0.042
C_{13}		1.144	2.098
C_{23}		1.170	2.098
C_{44}	2.4	3.452	3.250
C_{55}		3.201	3.250
C_{66}		3.297	3.973
C_{14}		0.015	
C_{15}		0.291	0.000
C_{16}		0.255	
C_{24}		−0.355	
C_{25}		0.090	0.000
C_{26}		0.073	
C_{34}		−0.029	
C_{35}		0.118	0.000
C_{36}		0.336	
C_{45}		0.007	
C_{46}		−0.011	0.000
C_{56}		−0.022	0.000
K_0	2.6	3.48	3.61
A	1.1	1.242	1.597

TABLE IX: Deviation of Proposed Symmetries of Doubly Relaxed Dodecasil-3C

space group			χ/Å	
symbol	no.	order	shell model	partial charge
$Fd\bar{3}$	203	24	0.488	0.268
$Fddd$	70	8	0.486	0.266
$R\bar{3}$	148	6	0.289	0.219
$C2/c$	15	4	0.264	0.000
$P\bar{1}$	2	2	0.000	0.000

space group; n = number of atoms in the unit cell; and N = number of symmetry operators in the space group. The structures that were relaxed only once (Dodecasil-3C$_o$, Dodecasil-3C$_t$, Dodecasil-3C$_o$) give χ values of about 0.0001 Å for their initial space groups. The only exception to this is the structure resulting from partial charge model relaxation of orthorhombic Dodecasil-3C, which has a χ value of 0.0137 Å for its original space group *Fddd* and 0.000 13 Å for its final space group $C2/c$. From Table IX one concludes that the doubly relaxed structure using the partial charge model (Dodecasil-3C$_5$) has $C2/c$ symmetry while the doubly relaxed structure using the shell model (Dodecasil-3C$_4$) has $P\bar{1}$ symmetry. The elastic constants of Dodecasil-3C$_5$ suggest a higher symmetry. The large decrease in symmetry, compared with the quasi-cubic structure that was used to start the relaxation, is due to the low symmetry of the added vibrational mode.

The experimental and theoretical values of the elastic anisotropy indicate that the clathrasil is nearly isotropic. This can be explained by the uniform directional distribution of the Si–O bonds, as can be seen in Table X, where the axes of the ellipsoids describing the bond direction distribution are given in combination with the elastic anisotropy. These ellipsoid axes are defined as the eigen vectors of the matrix **D** given by

$$\mathbf{D}_{\alpha\beta} = \sum_{i}^{n} \sum_{j \in \mathrm{nnb}_i} \vec{p}_\alpha^{ij} \vec{p}_\beta^{ij} \qquad (7)$$

with n = number of atoms; nnb$_i$ = set of nearest neighbors of atom i; $\vec{p}^{ij}$ = unit vector between atom i and j; and $\alpha, \beta = x, y, z$.

The eigen values, the lengths of the ellipsoid axes, are scaled by the largest one.

The phonon spectra of the doubly relaxed structures do not show imaginary frequencies, indicating that they represent stable energy minima.

The infrared spectra of Dodecasil-3C that are calculated with the shell model and partial charge model using the corresponding doubly relaxed structures Dodecasil-3C$_4$ and Dodecasil-3C$_5$

TABLE X: Si–O Bond Direction Distribution Ellipsoids

symmetry					
original	resulting[b]	potential	axes[a]		elastic anisotropy
cubic		unrelaxed	1.000	1.000	1.1[c]
	cubic	rigid ion	1.000	1.000	1.002
	cubic	shell	1.000	1.000	1.007
	cubic	partial charge	1.000	1.000	1.003
tetragonal		unrelaxed	0.997	1.000	1.1[c]
	cubic	rigid ion	1.000	1.000	1.002
	tetragonal	shell	0.994	1.000	1.645
	tetragonal	partial charge	0.998	0.998	1.710
orthorhombic		unrelaxed	0.991	0.992	1.1[c]
	cubic	rigid ion	1.000	1.000	1.002
	cubic	shell	1.000	1.000	1.086
	tetragonal	partial charge	0.999	0.999	1.597
cubic[d]	triclinic	shell	0.998	0.998	1.242
	monoclinic	partial charge	0.999	0.999	1.597

[a] Ellipsoid axes relative to longest axis. [b] Symmetry for which $\chi <$ 0.0001 Å. [c] Experimental value. [d] Double relaxed: Dodecasil-3C$_4$ and Dodecasil-3C$_5$.

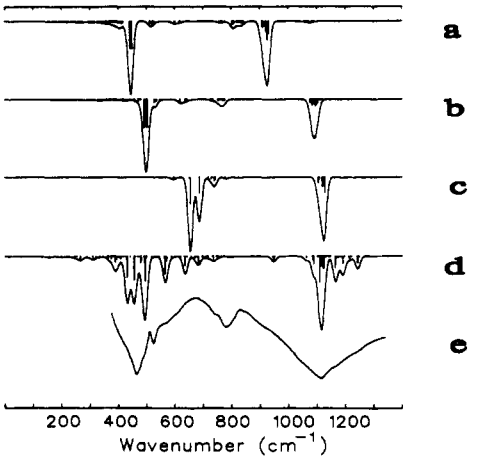

Figure 2. Infrared spectra of Dodecasil-3C: (a) shell model calculation on doubly relaxed Dodecasil-3C; (b) GVFF force field on doubly relaxed shell model Dodecasil-3C; (c) partial charge model calculation on doubly relaxed Dodecasil-3C; (d) GVFF calculation on doubly relaxed partial charge model Dodecasil-3C; (e) experiment.

(Figure 2) do not show an overall good agreement with the experimental spectrum. It was already known from previous studies[16,17] that the shell model gives only satisfactory results for the lower frequencies while the partial charge model is appropriate for calculating the higher part of the spectrum. These properties of the potentials are clearly reflected in the calculated spectra, but they hinder the use of the spectrum to determine which relaxed structure is best. Therefore the doubly relaxed structures have been used for a GVFF calculation using force constants derived by Etchepare[39] for α-quartz. The results are also given in Figure 2. Large differences between the two calculated spectra are found. On the basis of these results the triclinic structure predicted by the shell model has to be preferred. However, the GVFF calculation on the doubly relaxed shell model structure cannot account for the large width of the lines. Especially the width of the highest peak can indicate a large spread in the Si–O–Si angles[43] that is not reproduced by the shell model.

Table XI shows the results of calculations of the thermal ellipsoids of Dodecasil-3C$_4$ and Dodecasil-3C$_5$ using the shell model and partial charge model, respectively, together with data derived from the XRD experiment of Gies.[22] Because our main interest lies in the size and direction of the oxygen ellipsoids relative to the Si–Si bond, the ellipsoids are not presented in the usual **U**, **B** or **β** tensor form of anisotropic temperature factors but in terms of lengths of the ellipsoid axes and u_{SiSi}, the root mean square displacement of an oxygen atom in the Si–Si direction. All values

(43) van Santen, R. A.; Vogel, D. L. In *Advances in Solid-State Chemistry*; Catlow, C. R. A., Ed.; JAI: London, 1989; Vol. 1, p 151.

TABLE XI: Experimental and Calculated Thermal Ellipsoids (Doubly Relaxed Structures)

atom	experiment[22] axes/Å			u_{SiSi}[b]	shell[a] axes/Å			u_{SiSi}[b]	partial charge[a] axes/Å			u_{SiSi}[b]
Si1	0.146	0.161	0.174		0.075	0.080	0.089		0.078	0.084	0.087	
Si2	0.132	0.143	0.143		0.077	0.082	0.090		0.083	0.084	0.089	
Si3	0.134	0.134	0.134		0.080	0.085	0.094		0.087	0.090	0.090	
O1	0.138	0.278	0.305	47	0.079	0.127	0.169	48	0.080	0.125	0.142	61
O2	0.119	0.310	0.356	37	0.083	0.113	0.175	49	0.084	0.131	0.131	59
O3	0.114	0.240	0.304	45	0.083	0.134	0.163	51	0.085	0.120	0.168	65
O4	0.151	0.407	0.407	37	0.083	0.111	0.188	46	0.085	0.119	0.168	51

[a] Mean values are given (averaged per Wyckoff site of the atoms in the original cubic structure). [b] u_{SiSi} is the root mean square displacement of an oxygen atom in the direction of the line between the silicon atoms neighboring the oxygen atom. Its value is given as a percentage of the longest thermal ellipsoid axis.

TABLE XII: Convergence of Thermal Ellipsoid Calculation (Doubly Relaxed Shell Model Structure)[a]

atom	grid 3 × 3 × 3	6 × 6 × 6	9 × 9 × 9	unit
Si axis 1	0.0747 ± 0.0028	0.0755 ± 0.0028	0.0761 ± 0.0026	Å
Si axis 2	0.0800 ± 0.0024	0.0807 ± 0.0023	0.0811 ± 0.0022	Å
Si axis 3	0.0883 ± 0.0030	0.0888 ± 0.0030	0.0891 ± 0.0030	Å
O axis 1	0.0802 ± 0.0029	0.0808 ± 0.0029	0.0816 ± 0.0026	Å
O axis 2	0.1206 ± 0.0135	0.1210 ± 0.0134	0.1214 ± 0.0133	Å
O axis 3	0.1717 ± 0.0208	0.1720 ± 0.0207	0.1721 ± 0.0207	Å
O u_{SiSi}[b]	48.0 ± 5.4	48.3 ± 5.4	48.7 ± 5.5	%

[a] Mean values and root mean square deviations are given (averaged over all Si or O atoms in the triclinic unit cell). [b] u_{SiSi} is the root mean square displacement of an oxygen atom in the direction of the line between the silicon atoms neighboring the oxygen atom. Its value is given relative to the longest thermal ellipsoid axes.

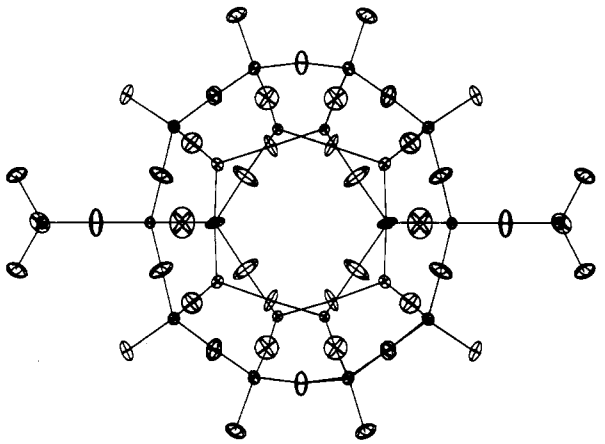

Figure 3. Ellipsoids given by experimental anisotropic temperature factors.[22]

are scaled with the length of the longest axis. It is clear that the experimental data show large anisotropic ellipsoids for the oxygen atoms with the main direction perpendicular to the Si–Si direction as indicated by the low u_{SiSi} values. The calculated ellipsoids are less anisotropic. Especially the u_{SiSi} values are much larger, indicating that the vibrations have less preference for directions perpendicular to the Si–Si direction. Table XII shows some averaged parameters of the calculated ellipsoids for three different integration grids in the case of the shell model. From this table, it can be concluded that the integration procedure converges. The thermal ellipsoids are drawn in Figures 3–5, superimposed on the respective experimental and doubly relaxed structures. Note that the ellipsoids are ellipsoids of thermal vibration and not the 50% probability ellipsoids usually drawn.[40,44] Figure 3 clearly displays the large thermal ellipsoid of the oxygen atom in the straight Si–O–Si bond (note that the bond is not in the projection plane). Figures 4 and 5 show the large decrease in symmetry of the doubly relaxed structures. Note that even with the magnification factor of 2 for the ellipsoids in Figures 4 and 5, the calculated ellipsoids are smaller than in the experiment. The ellipsoids for the oxygen

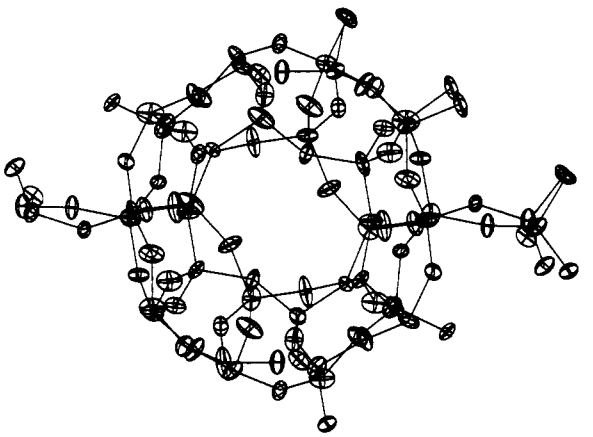

Figure 4. Thermal ellipsoids in the triclinic structure calculated by the shell model. Ellipsoids are magnified by a factor of 2.

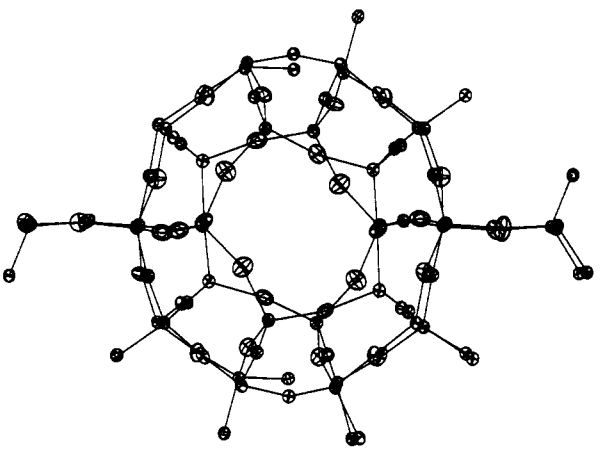

Figure 5. Thermal ellipsoids calculated by the partial charge model. Ellipsoids are magnified by a factor of 2.

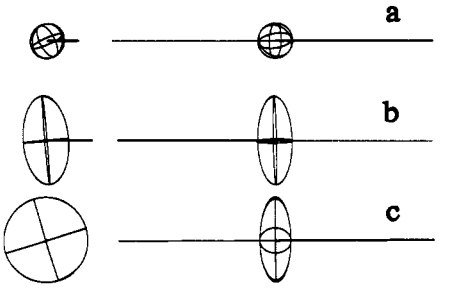

Figure 6. Thermal ellipsoid of the oxygen atom in the straight Si–O–Si bond in two projections (along the Si–Si line (left) and perpendicular to it (right)). The bonds are indicated by a line: (a) calculated by the partial charge model (magnified by a factor of 2); (b) calculated by the shell model (magnified by a factor of 2); (c) determined from experimental anisotropic temperature factors.

atom originally at the 180° Si–O–Si site are drawn in Figure 6, together with two Si–O bonds. The partial charge model gives

(44) Nelmes, R. J. *Acta Crystallogr. A* **1969**, *25*, 523.

TABLE XIII: T–O Distances for Straight and Bent T–O–T Bonds

structure	type	T–O distance/Å		Al/(Si + Al)	equiv Si–O distance/Å	
		T–O–T = 180°	T–O–T ≠ 180°		T–O–T = 180°	T–O–T ≠ 180°
Dodecasil-3C$_c$	MTN	1.536	1.570	0.0	1.536	1.570
Dodecasil-3C$_t$	MTN	1.536	1.570	0.0	1.536	1.570
Dodecasil-3C$_o$	MTN	1.589	1.601	0.0	1.589	1.601
Dachiardite[46]	DAC	1.597	1.629	0.22	1.573	1.604
Epistilbite[46]	EPI	1.572	1.623	0.262	1.544	1.594
Mordenite[46]	MOR	1.584	1.610	0.167	1.566	1.591
Ferrierite[46]	FER	1.592	1.609	0.163	1.574	1.591
Brewsterite[46]	BRE	1.585	1.645	0.25	1.558	1.617

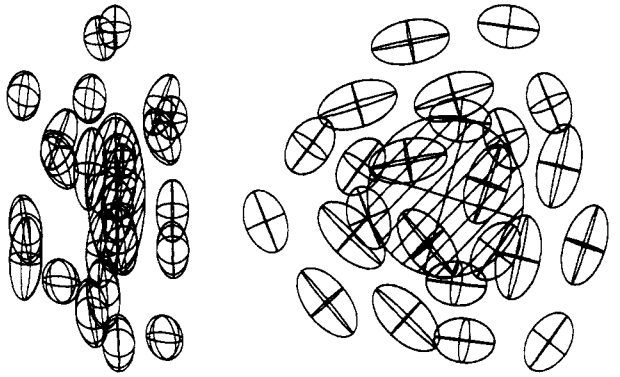

Figure 7. Calculated thermal ellipsoids of the oxygen atom in the experimentally straight Si–O–Si bond obtained by operating all symmetry elements of $Fd\bar{3}$ on the oxygen ellipsoid of the triclinic structure obtained by the shell model. The shaded region is the experimental ellipsoid. As in Figure 6 two projections are given: along the Si–Si line (left) and perpendicular to the bond (right).

an almost globular ellipsoid that is much smaller than the shell model one. This is probably due to the fact that the lower vibrational frequencies calculated by the partial charge model are too large due to the basis set used in the quantum chemical calculations on which the partial charge model is based.[17] Frequencies that are too high result in a systematical underestimation of the amplitudes of the vibrational displacement vectors. The absence of three-body interactions (bond bending terms) might even more lower the quality of the low-frequency part of the partial charge model spectrum. The shell model ellipsoid resembles the experimental ellipsoid better except for the projection perpendicular to the Si–Si line. This discrepancy is caused by a large static disorder contribution to the experimental ellipsoid and not by any preference of the oxygen vibration in a direction perpendicular to the Si–Si direction. This is illustrated by Figure 7 where all symmetry elements of the initial space group $Fd\bar{3}$ of the cubic crystal are operated on the shell model calculated ellipsoids of the oxygen atoms in the straight Si–O–Si bonds, giving an idea of how much disorder would be found by a structure refinement of the doubly relaxed shell model structure using $Fd\bar{3}$ as space group.

The simulated NMR spectrum of the doubly relaxed shell model structure shows a good agreement in the number of peaks with the experimental[45] spectrum of tetrahydrofuran–Dodecasil-3C at 213 K (Figure 8), while the doubly relaxed partial charge model structure corresponds to high-temperature (373 K) tetrahydrofuran–Dodecasil-3C. The exact location of the peaks, however, is not simulated very well. This is partially due to the very simple method used for calculating NMR shifts from structure, but there is also a large difference between Si–O–Si angles in the two calculated structures: the shell model structure has a mean Si–O–Si angle of 151.5° while the partial charge model structure shows a value of 169.6°. The experimental low-temperature spectrum shows a peak below the 180° limit of the simulation formula, indicating that a simple dependence of NMR shifts on Si–O–Si angles cannot describe all features of NMR spectra.

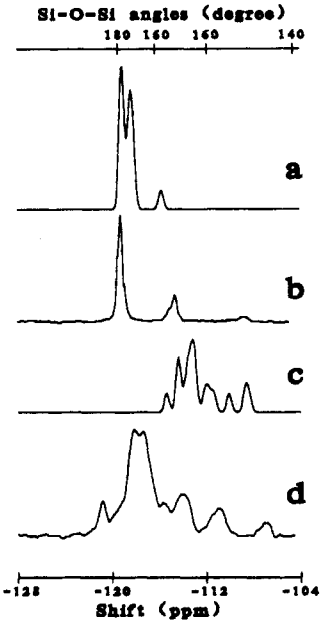

Figure 8. NMR spectra of Dodecasil-3C: (a) calculated from the doubly relaxed partial charge model structure using its Si–O–Si angle distribution; (b) obtained from experiment[45] at 373 K; (c) calculated from the doubly relaxed shell model structure using its Si–O–Si angle distribution; (d) obtained from experiment[45] at 213 K.

Discussion

The relaxation studies indicate that no Si–O–Si angle of 180° occurs in Dodecasil-3C. This agrees with earlier results by Alberti,[46] who found that five zeolites (Dachiardite, Epistilbite, Mordenite, Ferrierite, and Brewsterite) for which the original structure determinations indicated symmetry determined straight T–O–T angles (with T indicating Al or Si) lost these angles when a more accurate structure refinement was done using a lower symmetry. Another indication for the improbability of T–O–T angles of 180° is the low T–O distance for the atoms involved. Moving the oxygen atoms from the T–T line causes the T–O distance and the T–O–T angle to be more reasonable. This is illustrated by Table XIII, which contains the T–O distances for the atoms contributing to straight T–O–T angles compared with the mean values for the other atoms for the Dodecasil-3C structures under discussion and the zeolites used by Alberti. The zeolites in the table happen to have crystallographic sites for the T-atoms with equal aluminum occupancy per structure. This allows us to make a simple correction for the influence of the aluminum on the T–O distances in order to facilitate the comparison with the pure siliceous Dodecasil-3C. The mean Si–O bond length for silicates is 1.635 Å;[27] the mean Al–O distance is 1.75 Å[12]. Assuming that the AlO/SiO distance ratio is constant for any T–O bond in any topology, the correction takes the form

$$\langle \text{Si–O} \rangle = \frac{\langle \text{T–O} \rangle}{(1 - x + xf)} \qquad (8)$$

with ⟨T–O⟩ = mean T–O distance of the aluminum-containing structure; ⟨Si–O⟩ = mean Si–O distance of the aluminum-free

(45) Ripmeester, J. A.; Desando, M. A.; Handa, Y. P.; Tse, J. S. *J. Chem. Soc., Chem. Commun.* **1988**, 608.

(46) Alberti, A. *Proc. 7th Int. Zeolite Conf.*, Tokyo **1986**, 437.

structure; x = Al/(Al + Si) atomic ratio; and f = Al–O/Si–O distance ratio averaged over a large amount of aluminosilicates = 1.75/1.635. Both the real T–O distances and the corrected T–O distances ("Si–O" distances) are given in Table XIII.

In principle, the relation between T–O–T angle and T–O distance has a physical meaning that is discussed extensively in literature.[47-55] From a survey of experimentally determined Si–O distances in silica polymorphs, the following relation has been derived:[56]

$$\text{Si–O} = -0.068 \sec (\text{Si–O–Si}) + 1.526 \quad \text{Å} \qquad (9)$$

with a correlation coefficient r of 0.73 and an estimated standard deviation of 0.0034 Å for the slope. Although some deviations of the relation occur for high Si–O–Si angles, the Si–O distance at an angle of 180° can be estimated to be about 1.594 ± 0.0034 Å. An alternative description is given by Newton and Gibbs:[50]

$$\text{Si–O} = \frac{-0.319}{1 - \sec (\text{Si–O–Si})} + 1.754 \quad \text{Å} \qquad (10)$$

resulting in 1.59 Å for a straight angle. The distances for straight Si–O–Si angles in the structures of Table XIII are somewhat lower, but they are within the standard error values except for Dodecasil-3C. The clathrasil has low T–O distances for all T–O–T angles, and this cannot be explained by the absence of aluminum.

A definite determination of the symmetry of Dodecasil-3C cannot be given on the basis of the calculations presented. Since our calculations are essentially performed at 0 K, the prediction of the shell model calculation may correspond to the unknown low-temperature phase. The macroscopic observation of cubic symmetry can only be reconciled with our calculations and the NMR experiments mentioned above, both referring to observations on a microscopic level, if one assumes static disorder with local triclinic deformations resulting in a macroscopically cubic symmetry. The role of temperature effects can be elucidated by a free energy minimization.[18]

The method applied here of using vibrational modes with imaginary frequencies to generate new starting structures is very effective in speeding up the whole lattice minimization procedure. The check for the presence of imaginary frequencies should be used routinely to determine the stability of lattice energy minima. The disadvantages of the method is that it generally may result in low symmetry structures.

Thermal ellipsoid simulation can become a useful tool in powder XRD structure determinations since it can detect large static disorder contributions to experimental anisotropic temperature factors and help in deciding if the symmetry used in the structure refinement should be lowered.

Acknowledgment. We express our gratitude to Prof. H. Gies (Ruhr Universität Bochum) for providing a sample of Dodecasil-3C, to Prof. C. R. A. Catlow for useful discussions on the relaxation program, and to Dr. J. van Wolput (Eindhoven University of Technology) for measuring the infrared spectrum. This work is supported by the Dutch National Fund Supercomputers (NFS) of the SURF Foundation. The study is part of the EC project "Physical Chemistry of Zeolite Synthesis" (Project No. 88300423/JU1).

Registry No. SiO_2, 7631-86-9.

(47) Gibbs, G. V.; Meagher, E. P.; Smith, J. V.; Pluth, J. J. In *Molecular Sieves 2*; Kratzer, J. R., Ed.; ACS Symposium Series; American Chemical Society: Washington, DC, 1970; Vol. 40, p 19.
(48) Gibbs, G. V.; Hamil, M. M.; Louisnathan, S. J.; Bartell, L. S.; Yow, H. *Am. Mineral.* **1972**, *57*, 1578.
(49) Barrer, R. M. *Zeolites and clay minerals as sorbents and molecular sieves*; Academic Press: London, 1978.
(50) Newton, M. D.; Gibbs, G. V. *Phys. Chem. Minerals* **1980**, *6*, 221.
(51) Meagher, E. P.; Tossel, J. A.; Gibbs, G. V. *Phys. Chem. Minerals* **1979**, *4*, 11.
(52) Baur, W. H. *Acta Crystallogr. B* **1978**, *34*, 1751.
(53) Baur, W. H. *Acta Crystallogr. B* **1980**, *36*, 2198.
(54) Baur, W. H.; Ohta, T. *Acta Crystallogr. B* **1982**, *38*, 390.
(55) Tossel, J. A.; Gibbs, G. V. *Acta Crystallogr. A* **1978**, *34*, 463.
(56) Hill, R. J.; Gibbs, G. V. *Acta Crystallogr. B* **1979**, *35*, 25.
(57) Elcombe, M. M. *Proc. Phys. Soc. (London)* **1967**, *9*, 947.
(58) Kammer, E. W.; Atanasoff, J. V. *Phys. Rev.* **1942**, *62*, 395.